$\gamma^*\gamma^*$ Reactions at High Energies

A. Donnachie
Department of Physics and Astronomy, University of Manchester
Manchester M13 9PL, UK
email: ad@a3.ph.man.ac.uk

H.G.Dosch
Institut für Theoretische Physik der Universität Heidelberg
Philosophenweg 16, D-69120 Heidelberg
email: h.g.dosch@thphys.uni-heidelberg.de

M. Rueter[1]
School of Physics and Astronomy
Department of High Energy Physics, Tel Aviv University
69978 Tel Aviv, Israel
email: rueter@post.tau.ac.il

Abstract

The total hadronic $\gamma^*\gamma^*$ cross sections at high energy are calculated as a function of energy and photon virtuality in a model combining Reggeon exchange, the quark box diagram (a fixed pole in Regge language) and soft and hard pomeron exchanges evaluated in the context of dipole-dipole scattering. Good agreement is obtained with the data for the real $\gamma\gamma$ cross section and for the real photon structure function F_2^γ. However the model prediction for the $\gamma^*\gamma^*$ cross section is too small. This is attributed to an incorrect extrapolation of the Q^2 dependence of the hard pomeron adopted here. Parametrising it independently shows that the hard part of the cross section can be well represented by a simple Regge pole with intercept ~ 1.3.

[1]Supported by a MINERVA-fellowship

1 Introduction

The energy available for $\gamma^{(*)}\gamma^{(*)}$ physics at LEP2 is opening a new window on the study of diffractive phenomena, both non-perturbative and perturbative. These phenomena occur in each of untagged, single-tagged and double-tagged reactions via the total hadronic $\gamma\gamma$ cross section, $\sigma_{\gamma\gamma}$; the structure function of the real photon, F_2^γ (or equivalently the $\gamma^*\gamma$ cross section); and the total hadronic $\gamma^*\gamma^*$ cross section, $\sigma_{\gamma^*\gamma^*}$ respectively. Thus in principle it is possible to study diffraction continuously from the quasi-hadronic regime dominated by non-perturbative physics to the realm of perturbative QCD with either single or double hard scales. Although measurement of $\sigma_{\gamma^*\gamma^*}$ at high energies breaks new ground, data on F_2^γ at small x is equally significant. There has been considerable effort recently to understand the solution to the BFKL equation [1] in order to find the correct interpretation of the proton structure function at small x and large Q^2. As this has implications directly for F_2^γ at small x, and ultimately for $\sigma_{\gamma^*\gamma^*}$, it is worth summarising the current situation.

The leading order (LO) BFKL resummation [1] of the flavour singlet evolution equations was initially thought to provide a powerful tool for understanding the small-x limit of the proton structure function. It predicted the "hard pomeron", the structure function behaving as $\sim x^{-\lambda}$ with $\lambda \sim 0.5$ in conformity with the rapid rise with decreasing x discovered at HERA [2, 3]. However when the NLO corrections to the BFKL resummation were calculated [4, 5] the highest eigenvalue of the BFKL equation was found to be negative and large, so much so that it could lead to negative values of λ. It has been pointed out [6, 7] that this problem can be alleviated by identifying that part of the NLO corrections with double logarithms in the transverse momenta and resumming them. After ensuring the consistency of these double logarithms to all orders the perturbation series is much more convergent. The result in [7] is particularly stable and gives λ in the range 0.26 to 0.32 for the HERA kinematic regime. The double logarithms are closely associated with the choice of scale. It has been stressed [8] that the NLO corrections must necessarily contain both renormaliztion and scale ambiguities, and shown that the NLO corrections to the BFKL are controllable if appropriate renormalization scales and schemes are used, specifically the BLM [9] scheme for scale setting. In this approach the intercept of the NLO BFKL retains an extremely weak dependence on Q^2 and is smaller than the original BFKL intercept, having $\lambda \sim 0.2$ over the relevant experimental Q^2 range.

In the standard application of the DGLAP evolution equations [10] the rapid rise of the proton structure function at small x is associated with a singularity at $N = 0$ in the Mellin transform of the DGLAP splitting function. This singularity is not apparent in the original BFKL LO summation [1] nor in the NLO corrections of [6, 7]. It has been argued [11] that by analytically continuing in Q^2 one can conclude that the singularities in the complex N-plane of the Mellin transform of the proton structure function must also be present at small Q^2, and the perturbative evolution cannot generate new singularities that appear only at high Q^2. In this picture it is natural to associate the rapid rise of the proton structure function at small x with a second pomeron [12], very much in the spirit of the BFKL

approach. This hypothesis was successfully tested in [12], assuming that the contribution to the proton structure function from branch points is much weaker than that from poles and including only three of the latter: the standard reggeon and soft-pomeron exchanges known from purely hadronic interactions and a new hard pomeron with intercept $1 + \epsilon_0$. An excellent fit was obtained to the data for $x < 0.07$ and $0 \leq Q^2 \leq 2000$ GeV^2, giving $\epsilon_0 = 0.42$.

In references [1] and [4] through [8] the running of the coupling constant was not taken fully into account. A systematic approach to the BFKL equation at NLO with running coupling is presented in [13], adopting the BLM [9] scale-setting procedure. The effect is quite dramatic, removing all singularities to the right of $N = 0$ in the complex N-plane of the Mellin transform of the proton structure function i.e. there is no power-like behaviour at small-x from perturbative evolution. The solution factorizes into a part describing the evolution in Q^2 and a part describing the input distribution which is infrared dominated and non-calculable. Thus the BFKL equation can predict only the evolution in Q^2 of the structure function, the x dependence at small x being given partly by the evolution and partly by the input distribution. The evolution at small x differs significantly from that predicted from a standard NLO DGLAP treatment. A global fit to the proton structure function is very successful.

Thus we are currently in the position of having several apparently disparate views of small-x physics, and the quality of the corresponding fits to the $F_2(x, Q^2)$ data are such that the latter do not provide the necessary discrimination. Additional reactions are required, for example measurement of the proton longitudinal structure function $F_L(x, Q^2)$ or $\sigma_{\gamma^*\gamma^*}$ at high energies. We concentrate on the latter, with emphasis on the information which may be obtained from LEP. The advantage of $\gamma^*\gamma^*$ interactions is the absence of an initial non-perturbative state (e.g. the proton) and the presence of a hard component in the photon wave function, even for the real photon. Together these ensure that the "hard pomeron" plays a decisive rôle even at small virtualities. This has been demonstrated recently [14] for the real $\gamma\gamma$ cross section, the real photon structure function F_2^γ, and the reaction $\gamma^*\gamma^* \to V_1V_2$, where V_1, V_2 are any one of ρ, ω, ϕ, J/ψ.

The application of the BFKL formalism to $\gamma^*\gamma^*$ has been considerd by Brodsky et al [15] and by Boonekamp et al [16]. In the BFKL formalism there is a problem at LLO in setting the two mass scales on which the cross section depends: the mass μ^2 at which the strong coupling α_s is evaluated and the mass Q_s^2 which provides the scale for the high energy logarithms. Brodsky et al [15] argue that $\mu^2 \sim 10^{-1}Q_1Q_2$ and that $Q_s^2 \sim 10^2Q_1Q_2$ are reasonable choices. However the result is very sensitive to these parameters and by way of illustration they show that changing $\mu^2 \to 4\mu^2$ or $Q_s^2 \to Q_s^2/4$ alters the predicted cross section by factors of $\sim 1/4$ or ~ 4 respectively in a typical LEP experiment. In an attempt to overcome the scale problem, Boonekamp et al [16] take a phenomenological approach to estimate the NNLO effects, making use of a fit [17] to the proton sctructure function using the QCD dipole picture of BFKL dynamics. This reduces both the size of the BFKL cross scetion and its energy dependence.

The objective of this paper is to provide a realistic estimate of the known part of the cross section i.e. everything but the "hard pomeron" component although an estimate of that will also be given. There is a natural division of the contributions to the total cross section into quark-antiquark and multiple-gluon exchange in the t-channel. In terms of Regge-language the quark-antiquark exchange corresponds to that of a Reggeon and the gluon exchange corresponds to that of the Pomeron. In the language of structure functions the Reggeon exchange is mostly the valence quark contribution, the Pomeron exchange mostly the gluon contribution. Due to the different reference frames of the two approaches there is no strict one-to-one correspondence. The Regge language is applicable to photon-photon scattering for values of x sufficiently small, say $x \leq 0.1$, just as for deep inelastic scattering on nucleons. There is an important difference between hadron-hadron and photon-hadron or photon-photon scattering. To lowest order in QED there is no quadratic unitarity relation for the scattering amplitude and hence fixed singularities in the complex J-plane are possible and at least in one case (Compton scattering on hadrons) are required [18] - [20] by current algebra relations[21]. However this term is purely real and so does not contribute to the nucleon structure function F_2. In contrast, the box diagram in photon-photon scattering, which received much attention especially in the pre- and early QCD area (see [22] - [25] and the literature quoted therein) gives rise to a fixed J-plane singularity which does contribute to F_2^γ. This is an important point as it means that the valence-quark term and the box diagram must *both* be included as they correspond to different J-plane singularities.

It has been rather usual to approximate the soft-pomeron contribution to $\gamma^{(*)}\gamma^{(*)}$ scattering by assuming dominance of the vector meson resonances in the photon-channels. This is formally correct if all resonances are taken into account but that is impractical. Taking only one or two resonances into account can be misleading even at small virtuality, and furthermore the treatment of the longitudinal polarization of the photon is rather arbitrary. We therefore adopt an approach which considers the hadronic part of the photons as a superposition of quark-antiquark dipoles rather than vector mesons. In model investigations [26] it has been shown that this approach is much more economical since even for real photons the free photon wave function with a suitably chosen quark mass gives a more realistic description of a confined system than a superposition of many vector meson states. It is especially suited for treating the hard part of the photon, which in vector dominance can only be described by a superposition of infinitely many resonances. We thus expect, and obtain, large deviations from VMD.

The soft pomeron will be described by the interaction of the dipoles with the physical vacuum which has led to a satisfactory quantitative description of hadron-hadron scattering. For small dipole sizes its coupling is proportional to the product of the squares of the dipole radii and therefore is strongly suppressed for scattering of photons with high virtuality. The coupling of two perturbative gluons to small dipoles has a very different dependence on the radii which can be rather well described by:

$$\frac{R_1^2 R_2^2}{R_1^2 + R_2^2}.$$

Hence we anticipate, not unexpectedly, a strong dominance of perturbative effects if both photons are highly virtual. It turns out that for $\gamma^*\gamma^*$ scattering this virtuality need not be too high. Already for $Q_1^2, Q_2^2 \geq 5\text{GeV}^2$ there is clear evidence for the domination of the purely perturbative contribution.

The models are discussed in detail in Section 2, results are presented in Section 3 and final comments made in Section 4. At the end of Section 3 we present some simple fitting functions for the numerical results of our model.

We use the standard notation: $W = \sqrt{s}$ is the $\gamma^{(*)}\gamma^{(*)}$ c.m. energy; $Q_i^2 = -q_i^2$ are the photon virtualities. If one photon is on shell and one off shell we denote by Q^2 the virtuality of off shell photon and $x = \frac{Q^2}{s+Q^2}$.

2 The Model

2.1 The Pomeron Contribution

For the colour singlet exchange we use an eikonal approach [27] to high energy scattering particularly suited to incorporate non-perturbative aspects of QCD. The non-perturbative behaviour of QCD is treated in the Model of the Stochastic Vacuum [28, 29] which approximates the IR part of QCD by a Gaussian stochastic process in the colour field strength. This model yields linear confinent and can also be applied to high energy hadron-hadron scattering, or more generally to quark-antiquark dipole-scattering [30]. The model depends essentially on two typically non-perturbative parameters, which specify the Gaussian process mentioned above: the strength of the gluon correlator and a, the correlation length. These are related to the slope of the linear confining potential [28, 29]. As it stands the model leads to cross sections which are constant with increasing energy. The parameters of the model were fitted to the iso-singlet exchange part of (anti-)proton-proton scattering at $W = \sqrt{s}$= 20 GeV. The phenomenologically observed increase with energy of hadronic total cross sections like $s^{(\alpha_P - 1)}$ with $\alpha_P \approx 1.08$ [31] can be incorporated in two ways: either one lets the radius of the hadrons increase with s [30] - [33], or one takes the model as a determination of the Regge residue and adds the Regge-like increase with energy by a factor $(s/s_0)^{(1-\alpha_P)}$ with $\sqrt{s_0} = 20\text{GeV}$. These two approaches give very similar results, and we adopt the latter in this paper as it is the more convenient in the present context.

Whereas hadron-hadron scattering and soft electroproduction processes (i.e. those with low photon virtuality Q^2) can be very well described in this way, it is well known the energy dependence for hard electroproduction processes is much stronger than indicated by the soft non-perturbative pomeron. As discussed in the Introduction the occurence of a second (hard) pomeron as proposed in [12] can explain the data in a consistent way. This two pomeron approach was adapted to the MSV model in [34] and very successfully tested for the electro- and photoproduction of vector mesons and, more relevantly here,

for the proton structure function over a wide range of x and Q^2. As in [12] it was found that the soft-pomeron contribution to F_2, after an initial increase with increasing Q^2, has a broad maximum in the region of 5 GeV^2 and then decreases as Q^2 increases further i.e. it exhibits higher-twist like behaviour. In the context of the present model this is a consequence of the decreasing interaction strength with decreasing dipole size.

It is worth recalling the salient features of this version of the two-pomeron model, to illustrate the distinction between the soft and the hard pomeron in dipole-dipole scattering. In [34] it was assumed that all dipole amplitudes in which both dipoles are larger than the correlation length $a = 0.35$ fm are dominated by the soft pomeron, and the energy dependence therefore given by $(s/s_0)^{\alpha_{soft}-1}$ with $\sqrt{s_0} = 20$ GeV and $\alpha_{soft} = 1.08 + 0.25t$. This ensures that the hard pomeron has essentially no impact on purely hadronic scattering. If at least one of the dipoles is smaller than $a = 0.35$ fm then the trajectory is replaced by a fixed pole $\alpha_{hard} = 1.28$. This value was chosen as experimentally $F_2 \sim s^{0.28}$ at $Q^2 = 20\text{GeV}^2$ and the fixed-pole approximation made because of the lack of shrinkage in the J/ψ photoproduction cross section. It turned out that the model overestimated the non-perturbative contribution of very small dipoles so it was put to zero if either of the dipoles is less than 0.16 fm. With only four parameters it was possible to obtain a good description of data for the proton structure function and for the electroproduction of vector mesons without noticeably affecting earlier fits to hadron-hadron scattering.

We apply this two-pomeron model without change to the evaluation of the $\gamma^{(*)}\gamma^{(*)}$ cross sections. It should be noted that the simple factorisation formula $\sigma_{\gamma\gamma} = \sigma^2_{\gamma p}/\sigma_{pp}$ is no longer applicable in the two-pomeron situation.

The considerations outlined briefly above lead to a model for the scattering of quark-diquark dipoles on each other. In order to relate it to $\gamma^{(*)}\gamma^{(*)}$ interactions we have to introduce the photon wave function. In [26] it was shown by model considerations that the lowest-order perturbative expression for the quark-antiquark content of the photon, with chiral symmetry breaking and confinement being simulated by a Q^2-dependent quark mass, works remarkably well. The quark mass can be determined by comparing the result for the vector-current correlator with the analytically continued phenomenological expression in the Euclidean region. The resulting masses are:

$$\begin{aligned} m_{u,d} &= \begin{cases} m_0\,(1 - Q^2/1.05) & : \quad Q^2 \leq 1.05 \\ 0 & : \quad Q^2 \geq 1.05 \end{cases} \\ m_s &= \begin{cases} 0.15 + 0.16\,(1 - Q^2/1.6) & : \quad Q^2 \leq 1.6 \\ 0.15 & : \quad Q^2 \geq 1.6 \end{cases} \\ m_c &= 1.3 \end{aligned} \tag{1}$$

The parameter m_0 for the u, d quarks was found to be $m_0 = 0.21 \pm 0.015$ GeV.

2.2 The Box Diagram

For Compton scattering on hadrons it was shown in [18] - [20] that the Fubini-Dashen-Gell-Mann sum rules which relate the integral over the imaginary part of the Compton amplitude to the electromagnetic form factor $F(t)$ lead under very general assumptions to a fixed (i.e. t-independent) pole in the complex J-plane whose residue is proportional to $F(t)$. The residue is real and hence cannot contribute to the structure function. Such a fixed J-plane singularity also occurs in photon-photon scattering due to the box diagramm. The large-s behaviour of it is independent of the momentum transfer and the virtuality and is of the order $i \log s$ which corresponds to a fixed double pole. For very large virtualities of the photons or high quark masses the QCD corrections to the box diagram are under control [25] and it should not be modified by them in any essential way. It is thus natural to add the contribution of the box diagram representing this J-plane singularity to the valence quark contributions corresponding to the Reggeon exchange without conceptual difficulties of double counting. The singularity contributes to the imaginary part of the residue and we have a contribution to the gamma-gamma cross section $\sigma^{box}_{\gamma^*\gamma^*} = \text{const} \ \times \log(s)/s$.

We give here the full cross section for $\gamma^{(*)}\gamma^{(*)}$ scattering for a colour triplet of quarks with mass m and charge $e_f = \hat{e}_f \cdot e$:

$$\begin{aligned}
\sigma(W^2, Q_1^2, Q_2^2) = &-\frac{3\pi}{2}\hat{e}_f^4\alpha^2\frac{|\vec{p}|}{|\vec{q}|W^2} \qquad (2)\\
&\times\left(8+\frac{4\ (2\,m^2-Q_2^2)\ (2\,m^2-Q_1^2)}{|\vec{p}|\,|\vec{q}|\ (Q_2^2-4\,|\vec{p}|\,|\vec{q}|+Q_1^2+W^2)}-\frac{4\ (2\,m^2-Q_2^2)\ (2\,m^2-Q_1^2)}{|\vec{p}|\,|\vec{q}|\ (Q_2^2+4\,|\vec{p}|\,|\vec{q}|+Q_1^2+W^2)}\right.\\
&+\frac{2\ (-8\,m^4+Q_2^4+2\,Q_2^2\,Q_1^2+Q_1^4+W^4+4\,m^2\ (Q_2^2+Q_1^2+W^2))}{|\vec{p}|\,|\vec{q}|\ (Q_2^2+Q_1^2+W^2)}\\
&\left.\times\log(\frac{Q_2^2-4\,|\vec{p}|\,|\vec{q}|+Q_1^2+W^2}{Q_2^2+4\,|\vec{p}|\,|\vec{q}|+Q_1^2+W^2})\right)
\end{aligned}$$

with

$$|\vec{p}| = \sqrt{-m^2+\frac{W^2}{4}}, \qquad |\vec{q}| = \frac{\sqrt{Q_2^4-2\,Q_2^2\,Q_1^2+Q_1^4+2\,Q_2^2\,W^2+2\,Q_1^2\,W^2+W^4}}{2\,W}.$$

If $m_q^2 \ll Q_1^2 \ll W^2$ and $Q_2^2 \ll m_q^2$ we have:

$$\sigma_{\gamma^*\gamma^*} = 4\pi^2\alpha^2 F_2^\gamma = 12\pi\alpha^2\left(\sum_f \hat{e}_f^2\right)^2\frac{1}{W^2}\left(\log\frac{W^2}{m_q^2}-1\right).$$

For the case: $0 \ll Q_1^2, Q_2^2 \ll W^2$ we have:

$$\sigma_{\gamma^*\gamma^*} = 4\pi^2\alpha^2 F_2^\gamma = 12\pi\alpha^2\left(\sum_f \hat{e}_f^2\right)^2\frac{1}{W^2}\left(\log\frac{W^4}{Q_1^2\,Q_2^2}-1\right).$$

If at least one of the photon virtualities is smaller than the internal quark mass the box diagram receives important contributions from the IR region and thus depends crucially on the quark mass. In our approach it is natural to use therefore for small Q^2 the same Q^2-dependent quark mass as in the photon wave function (see equation 1).

2.3 The Reggeon

In many respects the contribution from the coupling of the reggeon to the hadronic content of the photon (ρ, ω, ϕ etc.) is the least well-defined. Even with one photon on-shell, i.e. for the valence quark contribution $F^{\gamma}_{2,had}$ to the hadronic structure function of the real photon, there are considerable ambiguities [35, 36, 37]. In naive Vector Meson Dominance (VMD) this is given by

$$\frac{1}{\alpha}F^{\gamma}_{2,val}(x,Q^2) = F^{\pi}_{val}(x,Q^2)\sum_V \frac{4\pi}{f_V^2}, \tag{3}$$

where the sum is usually over ρ, ω and ϕ. The additional assumption has been made that the vector meson structure functions can all be represented by the valence structure function of the pion $F^{\pi}_{val}(x,Q^2)$. This in itself is quite an extreme statement, as there is no obvious reason why the structure function of the short-lived vector mesons should be the same as those of the long-lived pion. Additionally it is not clear whether one should take the simple incoherent sum or allow for coherence effects. Finally, higher-mass vector mesons must also make some contribution, but this is almost certainly small for the real photon as compared to the uncertainties in any estimate of the hadronic component.

To add to these uncertainties, the pion structure function is only known experimentally for $x > 0.2$. To obtain the structure function in the kinematical domain of interest here, it is necessary to use the DGLAP evolution equations to fit the data and to extrapolate [38, 39]. This was the approach used by [35, 36] in fitting F_2^{γ}, although with somewhat different assumptions about the effective strength of the contribution. In contrast, in [37] the shape of the hadronic contribution was left free to be determined by the data, but the normalisation was fixed.

In our previous work [14] we used the DGLAP evolved pion structure function of [39], and retained only the ρ, ω and ϕ in the sum of eqn.(1). At small x ($x \leq 0.1$) and small Q^2 ($Q^2 \leq 25\mathrm{GeV}^2$) this can be well parametrised by

$$F_{2,val} = C(\frac{Q^2}{Q^2+a})^{1-\eta}x^{\eta} \tag{4}$$

with $a = 0.3$ GeV^2, $C = 0.38$ and $\eta = 0.45$. Thus for the valence quark contribution to the $\gamma^*\gamma$ cross section we get

$$\sigma_{\gamma^*\gamma}(s,Q^2) = 4\pi^2\alpha^2\frac{C}{s}(\frac{s}{Q^2+a})^{1-\eta} = \frac{312}{s}(\frac{s}{Q^2+0.3})^{0.55}\text{nb}. \quad (5)$$

This simple formula holds to better than 10% over the (x,Q^2) range relevant for LEP. That is the error is much less than the other uncertainties in estimating this term.

Extrapolating eqn.(3) to $Q^2 = 0$ does not satisfy simple factorisation. The total γp and pp ($p\bar{p}$) cross sections can be described by three terms corresponding to soft pomeron exchange, $C = +1$ reggeon exchange and $C = -1$ reggeon exchange, with universal powers of s for each. In the absence of cuts (and the universality implies that these should be small) each term should factorise independently. That is

$$\sigma^i_{\gamma\gamma} = \frac{(\sigma^i_{\gamma p})^2}{\sigma^i_{pp}} \quad (6)$$

where i corresponds to any one of the soft pomeron, $C = +1$ reggeon or $C = -1$ reggeon contributions. The value of η used in eqns.(2) and (3) corresponds to the fit to total cross sections of [31], from which one finds

$$\sigma^{C=+1}_{\gamma\gamma} = 216 s^{-\eta}\text{nb} \quad (7)$$

which is about $\frac{1}{3}$ of eqn.(3) in the $Q^2 \to 0$ limit. If one applies factorisation to the latest PDG fit [40] to total cross sections then the result is approximately midway between these two extremes although with a somewhat different energy dependence. Thus it seems reasonable, given all the uncertainties, to take eqns.(3) and (5) as giving upper and lower limits respectively to the reggeon exchange contribution to the total hadronic $\gamma\gamma$ cross section.

The simplest approach to extending eqn.(3) to the case when both photons are off-shell is to assume that as it is a reggeon contribution it should factorise:

$$\sigma_{\gamma^*\gamma^*}(s,Q_1^2,Q_2^2) = 4\pi^2\alpha^2\frac{C}{a}(\frac{a}{Q_1^2+a})^{1-\eta}(\frac{a}{Q_2^2+a})^{1-\eta}(\frac{s}{a})^{-\eta}\text{nb}. \quad (8)$$

with C and a having the same values as before.

3 Results

The pomeron contribution to $\sigma_{\gamma\gamma}$is rather sensitive to the effective light-quark mass m_q entering the photon wave function, varying as $\sim 1/m_q^4$. This is illustrated in Figs.(1a) and (1b) which show separately the L3 [41, 42] and OPAL [43, 44] data and the pomeron model with $m_q = 210$ MeV and 200 MeV respectively, together with the other contributions to

the total cross section. These values of m_q are slightly lower than the 220 MeV used in the earliest calculations, but have no observable effect on the purely hadronic predictions of the model and actually serve to improve slightly the description of high-energy photon-proton reactions [26, 45]. They are also within the expected range of 210 ± 15 MeV, as determined from the two point vector function [26]. The sensitivity to m_q disappears once $Q^2 \gg m_0^2$.

It is clear that the hard part of the pomeron contribution becomes increasingly important with increasing energy, reaching more than 20% of the cross section at a c.m. energy of 130 GeV. This relatively strong fraction of the hard part is a consequence of the pointlike coupling of the photons to the quarks and the resulting singularity at zero distance of the photon wave function. In the corresonding picture for proton-antiproton scattering the hard part is only about 1% of the cross section at $W = 130$ GeV.

The predictions of the same model for the $\gamma^*\gamma^*$ cross sections at $Q^2 = 3.5$ GeV^2 and 14 GeV^2 are compared with the recent L3 data [46] in Table 1 and shown in Fig.2. The predictions at $Q^2 = 3.5$ GeV^2 are slightly below and at 14 GeV^2 distinctly below the data, especially at the higher values of W. This and the many successful tests of the soft pomeron part within the model make it very likely that the discrepancy is due to a wrong Q^2 dependence of the hard part. Therefore in Fig.3 we plot the difference between experiment and the sum of soft pomeron and non-diffractive terms. This difference represents the hard part of the reaction. It is interesting that at all virtualities the data can be fitted well with a power behaviour $W^{2\epsilon} = s^\epsilon$ with $\epsilon \sim 0.3$, fully consistent with a hard second pomeron. Of course the error on ϵ is large ~ 0.1. The comparatively small contribution to the cross section from the soft pomeron is directly attributable to its decreasing interaction strength with decreasing dipole size (the higher-twist behaviour) found in deep inelastic scattering [12, 34].

We can easily see why the model with parameters taken from the nucleon structure functions can fail when applied to the $\gamma^*\gamma^*$ cross section. In Table 2 we give the power dependence on the dipole size R, and correspondingly Q^2, of different terms: perturbative two gluon exchange: the genuine non-perturbative contribution: and the contribution of (naive) vector meson dominance. We see that for one dipole large (e.g. the nucleon in the structure functions) the Q^2 behaviour is the same for the total pomeron contribution in the model and the perturbative two-gluon exchange. Therefore a distinction between the two is difficult. However this is not the case when the two dipoles become small. Here the perturbative two-gluon exchange falls off much slower with decreasing dipole size (increasing Q^2) than does the pomeron contribution in the model. It is therefore very plausible that the residue of the hard pomeron has a Q^2 dependence more akin to that of the perturbative contribution rather than to the nonperturbative term (as implied in the present model [34]).

If this explanation is correct then the present model should still give a good description of the structure function of the real photon, F_2^γ, as the real photon is dominated by a large dipole size. It is similar to, but not exactly the same as, the nucleon structure function

W	L3	F.P.	R.P.	S.P.	H. Ex.	Error	H. Mod.
$Q^2 = 3.5$							
6.5	27	13.1	6.8	0.7	6.3	5	1.4
10.8	20	9.8	4.3	1.1	4.8	3.5	2.2
22.8	21	3.8	2.2	2.	13.0	4.5	4.1
$Q^2 = 14$							
13	7.2	3.5	0.9	0.02	2.8	2.5	0.32
21.6	7.2	2.7	0.5	0.04	3.9	2.5	0.48
45.6	8.2	1.1	0.3	0.07	6.8	3.5	0.87
$Q^2 = 14.5$							
13.3	7.5	3.4	0.8	0.02	2.5	1.3*	0.30
21.9	7.3	2.6	0.5	0.03	4.17	1.3*	0.48
36.1	5.5	1.5	0.3	0.05	3.65	1.5*	0.68
56.6	7.4	0.8	0.2	0.08	6.3	2.3*	0.99

Table 1: $\gamma^*\gamma^*$ total cross section in nb. W: $\gamma^{(*)}\gamma^{(*)}$ c.m. energy [GeV]; L3: experimental results from L3 [41, 46]; F.P.: fixed pole (box-diagram); R.P.: reggeon-contribution (valence term); S.P.: soft pomeron (non-perturbative contribution); H.Ex: hard 'experimental' contribution: Error: experimental error; H.Mod: hard contribution extrapolated from the model adapted to the proton structure function [34].

but is not precisely analogous as the real photon has a small-dipole component not present in the nucleon. The predictions of the model are compared with F_2^γ data in Fig.4. They extend to larger x than in our previous work [14] because of the inclusion of the box diagram which we omitted previously : $x \leq \min(0.2, Q^2/(25+Q^2)$, i.e $W \geq 5$ GeV. The agreement with experiment is indeed very satisfactory stressing again the reliability of the model if at least one of the dipoles is large. Figure 5 shows the smooth extrapolation from the purely perturbative domain ($Q^2 = 0$) to the domain of DIS. It can be seen from the prediction for $W = 50$ GeV that at that energy the hard pomeron is dominant even at

	Non-pert.	Pert.	naive VDM
2 dipoles small:	$R_1^2 \cdot R_2^2$ $\frac{1}{Q_1^2 \cdot Q_2^2}$	$R_1 \cdot R_2$ $\frac{1}{Q_1 \cdot Q_2}$	$\frac{1}{Q_1^4 \cdot Q_2^4}$
1 dipole small:	R_i^2 $\frac{1}{Q_i^2}$	R_i^2 $\frac{1}{Q_i^2}$	$\frac{1}{Q_i^4}$

Table 2: Behaviour of the different contributions leading in W to the $\gamma^*\gamma^*$ cross section (up to logarithmic terms).

moderate virtualities. This stresses the relevance of F_2^γ as data can be taken at smaller x (higher W) and larger Q^2 than for the $\gamma^*\gamma^*$ cross section, so it remains a sensitive probe of the hard pomeron.

Table 2 demonstrates that the model shows a significant deviation from simple VMD at large Q^2, and this is still valid at small Q^2. A comparison of the model and naive VMD is made in Fig.5 which shows the ratio of the model cross section to the VMD cross section as a function of Q^2, normalised to one at $Q^2 = 0$. The two plots are for the two centre of mass energies of the $\gamma^*\gamma^*$ system $W = 90$ GeV and $W = 245$ GeV.

This deviation from naive VMD is of particular importance in the present evaluation of the real photon cross section, $\sigma_{\gamma\gamma}$, as the data are untagged and cover a finite range of Q^2. The normal procedure is to assume VMD to extract $\sigma_{\gamma\gamma}$, but our results indicate that this is not reliable. We fitted our results for the total $\sigma_{\gamma^*\gamma^*}$ cross section in the kinematical range $90 < W < 250$ GeV and $0 < Q_i^2 < 3$ GeV^2 with an ansatz which shows explicitly the deviation from the naive VMD behaviour for the Q^2 dependence and for fixed virtualities it is a simple power fit for the W-dependence:

$$\begin{aligned}\sigma_{\gamma^*\gamma^*} &= \left(a + \left(b + c * Q_1^2\right)\right) * \exp\left(-d * Q_1^2\right) * \left(a + \left(b + c * Q_2^2\right)\right) * \exp\left(-d * Q_2^2\right) \\ &\quad * 1/\left(Q_1^2 + m_\rho^2\right) * 1/\left(Q_2^2 + m_\rho^2\right) \\ &\quad * (W/20\text{ GeV})^{\left(e + f * Q_1^2 * \exp\left(-g * Q_1^2\right)\right) * \left(e + f * Q_2^2 * \exp\left(-g * Q_2^2\right)\right)} \ . \end{aligned} \tag{9}$$

Our fit for the seven parameters a-g results in (Q_i^2 in GeV^2, W and m_ρ in GeV, $\sigma_{\gamma^*\gamma^*}$ in nano-barns)

$$a = 9.10, b = 0.398, c = 3.380, d = 0.541, e = 0.554, f = 0.115, g = 0.276 \ . \tag{10}$$

For convenience we give also fitting formulae for the case of one real and one real or virtual photon as obtained in the model applicable in the range 10 GeV $\leq W \leq$ 150 GeV and $0 \leq Q^2 \leq 25$ GeV^2 by the following expressions (W in GeV, Q^2 in GeV^2):

$$\sigma_{\gamma^{(*)}\gamma}(W, Q^2) = \frac{1}{(Q^2 + 0.6)} * \left(A_0(Q^2) + A_1(Q^2)\ \log(W/20) + A_2(Q^2)\ (\log(W/20))^2\right) \tag{11}$$

For the soft pomeron contribution we have:

$$\begin{aligned} A_0 &= \frac{724.6}{Q^2 + 5.31} \\ A_1 &= \frac{142.9}{1.666 + 3.114\exp(-Q^2) + \sqrt{Q^2}} \\ A_3 &= 1.11\sqrt{Q^2} + 0.0311 \end{aligned}$$

For the hard pomeron:

$$A_0 = 95.67 - \frac{148.15}{Q^2 + 1} + \frac{79}{(Q^2 + 1)^2}$$

$$A_1 = 68.66 - \frac{116.9}{Q^2+1} + \frac{66.6}{(Q^2+1)^2}$$
$$A_3 = 31.83 - \frac{75}{Q^2+2} + \frac{11.45}{(Q^2+1)^2}$$

From this expression one obtains the photon structure function for $Q^2 \neq 0$:

$$\frac{1}{\alpha} F_2^\gamma(x,Q^2) = \frac{Q^2}{4\pi\alpha^2}\sigma_{\gamma^{(*)}\gamma}(W,Q^2) \tag{12}$$

The expressions for the fixed pole (box) and reggeon are given analytically through equations (2) and (8) respectively.

4 Summary

The most significant result is that a well-tried model of diffraction which successfully describes high-energy hadronic interactions, vector meson production, deep inelastic scattering at small x, the real $\gamma\gamma$ cross section and the structure function of the real photon fails to predict correctly the $\gamma^*\gamma^*$ cross section even at quite modest photon virtuality of $\langle Q^2 \rangle = 14.0$ GeV^2. This is clearly due to the fact that, uniquely among these various processes, the $\gamma^*\gamma^*$ interaction involves two small dipoles, and emphasizes the importance of the $\gamma^*\gamma^*$ cross section as a probe of the dynamics of the perturbative hard pomeron. If the genuinely non-perturbative terms i.e. the soft phenomenological pomeron and Reggeon exchange, together with the box diagram are subtracted from the $\gamma\gamma$ and $\gamma^*\gamma^*$ data then the results can be fittedwith a single power energy dependence s^ϵ with $\epsilon = 0.3 \pm 0.1$. The errors on ϵ are large, partly because of the errors on current data and partly because of the considerable uncertainty in the Reggeon term. Given the rather low values of $W_{\gamma^*\gamma^*}$ accessible to LEP at the higher values of Q^2 it is clearly important to get a much better understanding of the Reggeon term than we have at present.

We have noted that the model works very well for the real $\gamma\gamma$ cross section and for the real photon structure function due to the presence of two, respectively one, large dipoles. Of course the real photon is not a hadron, with the consequence that there is an important contribution in the model from the hard pomeron to the real $\gamma\gamma$ cross section. However it has to be added that this is, as yet, not strictly required by the data. Clarification of the remaining discrepancies between L3 and OPAL would help, as would better data at lower energies enabling the Regge term to be more tightly constrained. The importance of the hard pomeron is even more marked in the case of the real photon structure function, although data are not yet at sufficiently small x for the hard pomeron to dominate. Data for $x \leq 10^{-2}$ and $Q^2 \geq 10$GeV^2 should clearly show its presence.

Finally we have shown that, within the model, the $\gamma^*\gamma^*$ cross section at small Q_1^2, Q_2^2 decreases less quickly with increasing Q^2 than is impled by naive Vector Meson Domi-

nance. As the model underestimates the cross section at larger Q^2 it is likely that the effect at small Q^2 is more marked than we have indicated. As the real $\gamma\gamma$ cross section is obtained at present by extrapolating from non-zero Q^2 using Vector Meson Dominance it is probable that it is significantly over-estimated.

References

[1] V.S.Fadin, E.A.Kuraev and L.N.Lipatov: Phys.Lett. **60B** (1975) 50
Y.Y.Balitskii and L.N.Lipatov: Sov.J.Nucl.Phys. **28** (1978) 822

[2] C.Adloff et al: Nucl.Phys. **B497** (1997) 3

[3] J.Breitweg et al: Z.Phys. **C75** (1997) 215

[4] V.S.Fadin and L.N.Lipatov: Phys.Lett **B429** (1998) 127

[5] M.Ciafaloni and G.Camici: Phys.Lett. **B430** (1998) 349

[6] G.P.Salam: hep-ph/9806482 v2

[7] M.Ciafaloni and D.Colferai: hep-ph/9812366

[8] S.J.Brodsky, V.S.Fadin, V.T.Kim, L.N.Lipatov and G.B. Pivovarov hep-ph/9901229

[9] S.J.Brodsky, G.P.Lepage and P.B.Mackenzie: Phys.Rev **D28** (1983) 228

[10] V.N.Gribov and L.N.Lipatov: Sov.J.Nucl.Phys. **15** (1972) 438 and 675
L.N.Lipatov: Sov.J.Nucl.Phys. **20** (1975) 94
Yu.L.Dokshitser: Sov.J.JETP **46** (1977) 641
G.Altarelli and G.Parisi: Nucl.Phys. **B126** (1977) 298

[11] J.R.Cudell, A.Donnachie and P.V.Landshoff: hep-ph/9901222; Phys.Lett **B**, in press

[12] A.Donnachie and P.V.Landshoff: Phys.Lett. **B437** (1998) 408

[13] R.Thorne: hep-ph/9901331

[14] A.Donnachie, H.G.Dosch and M.Rueter: hep-ph/9810206; Phys.Rev. **D**, in press

[15] S.J.Brodsky, F.Hautmann and D.E.Soper: Phys.Rev. **D56** (1997) 6957

[16] M.Boonekamp, A.De Roeck, C.Royon and S.Wallon: hep-ph/9812523

[17] A.Bialas, R.Peschanski and C.Royon: Phys.Rev. **D57** (1998) 6899
H.Navelet, R.Peschanski and C.Royon: Nucl.Phys. **B534** (1998) 297

[18] J.B. Bronzan, I.S.Gerstein, B.W.Lee, and F.E.Low: Phys.Rev.Lett. **18** (1967) 32

[19] J.B.Bronzan, I.S.Gerstein, B.W.Lee, and F.E.Low: Phys.Rev. **157** (1967) 1448

[20] V.Singh: Phys.Rev.Lett **17** (1967) 340

[21] S.Fubini: Nuovo Cim.**43** (1966) 475

[22] R.P.Feynman: Phys.Rev.Lett. **23** (1969) 1415

[23] H.Terazawa: Rev.Mod.Phys. **45** (1973) 2105

[24] E.Witten: Nucl.Phys. **B120** (1977) 189

[25] C.T.Hill and G.Ross: Nucl.Phys. **B148** (1979) 373

[26] H.G.Dosch, T.Gousset and H.J.Pirner: Phys. Rev. **D57** (1998) 1666

[27] O.Nachtman: Ann.Phys. **209** (1991) 436

[28] H.G.Dosch: Phys.Lett. **B190** (1987) 555

[29] H.G.Dosch and Yu.A.Simonov: Phys.Lett. **B205** (1988) 339

[30] H.G.Dosch, E.Ferreira and A.Krämer: Phys.Rev. **D50** (1994) 1992

[31] A.Donnachie and P.V.Landshoff: Phys.Lett. **B296** (1992) 227

[32] E. Ferreira and F. Pereira, Phys. Rev. **D55** (1997) 130; ibid **D56** (1997) 179

[33] E.R. Berger and O. Nachtmann, hep-ph/9808320

[34] M.Rueter: hep-ph/9807448; Eur.Phys.J. **C**, in press

[35] M.Glück, E.Reya and A.Vogt: Phys. Rev. **D46** (1992) 1973

[36] P.Aurenche, M.Fontannaz and J.Ph.Guillet: Z.Phys. **C64** (1994) 621

[37] G.A.Schuler and T.Sjöstrand: Z.Phys. **C68** (1995) 607

[38] P.Aurenche: Phys. lett. **B233** (1989) 517

[39] M.Glück, E.Reya and A.Vogt: Z.Phys. **C53** (1992) 651

[40] Particle Data Group: European Physical Journal **3** (1998), page 205

[41] L3 Collaboration: M.Acciari et al: Phys. Lett. **B408** (1997) 450
L3 Collaboration: L3 Note 2280: Submitted to *XXIX ICHEP*, Vancouver, 1998

[42] L3 Collaboration: M.Acciari et al. L3 Note 2400 *Int. Europhys. Conf. 99*

[43] OPAL Collaboration: F.Wäckerle: *Proc. XXVIII Int. Symp. on Multiparticle Dynamics*, Frascati, 1997

[44] OPAL Collaboration: G. Abbiendi et al., to be submitted to Europ. Phys. J. C

[45] G.Kulzinger, H.G.Dosch and H.J.Pirner: Eur.Phys.J. **C** (to be published)

[46] L3 Collaboration: M.Acciari et al: Phys.Lett. **B453** (1999) 333 and L3 Note 2404

[47] L3 Collaboration: M.Acciari et al: Phys.Lett. **B436** (1998) 403 and Phys.Lett. **B447** (1999) 147

[48] OPAL Collaboration: K.Ackerstaff et al.: Phys.Lett. **B411** (1997) 387 and Phys.Lett. **B412** (1997) 225

[49] OPAL Collaboration: OPAL Physics Note PN389 (Preliminary)

[50] ALEPH Collaboration: R.Barate et al.: Phys. Lett. **B458** (1999) 152

[51] ALEPH Collaboration: ALEPH 99-038: EPS-HEP99 Conference, Tampere

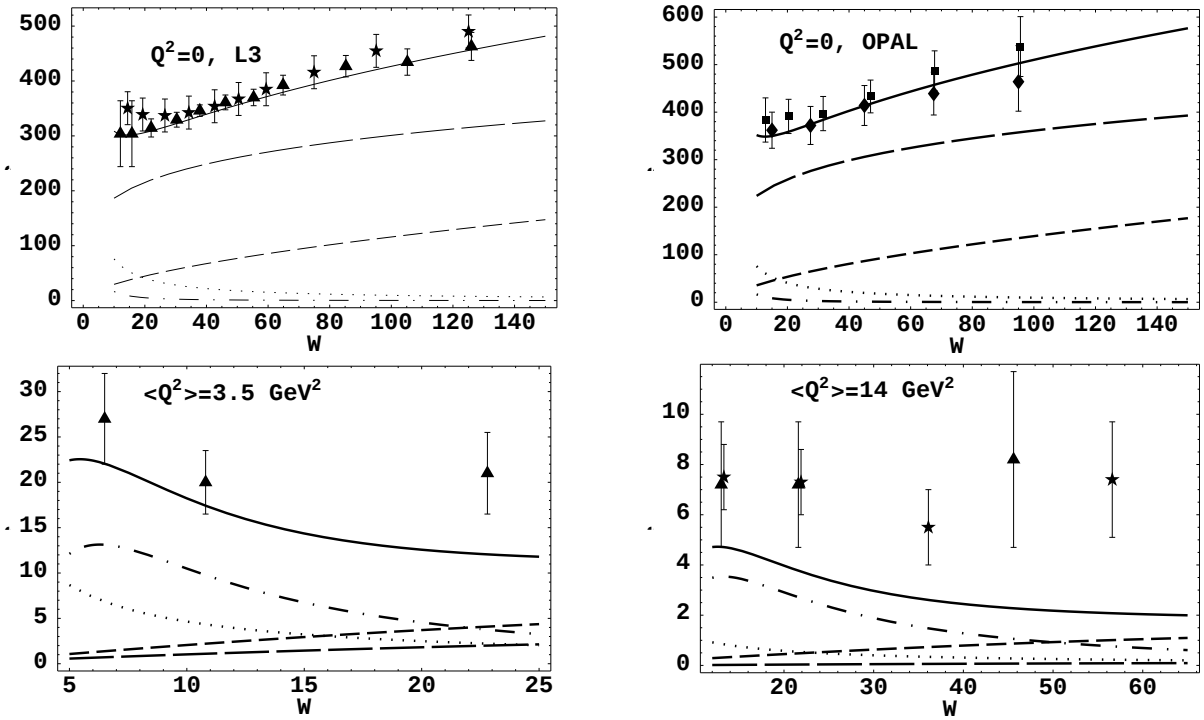

Figure 1: Cross sections in nb for $\gamma^{(*)}\gamma^{(*)}$ scattering for virtualities $Q^2 = 0$, 3.5 and 14 GeV^2 respectively compared with OPAL and L3 data. L3 [41, 46], Triangles; L3 [42] and private communication, Stars: OPAL [43], Boxes ; OPAL [44], Diamonds. The solid curve is our model . It consists of the following contributions: soft pomeron: long dashes; hard pomeron: short dashes; fixed pole (box): dot-dashes; reggeon: dots. For the L3 data a Q^2-dependent quark mass with $m_0 = 0.21$ GeV was used, for the OPAL data $m_0 = 0.20$ GeV, see equation (1).

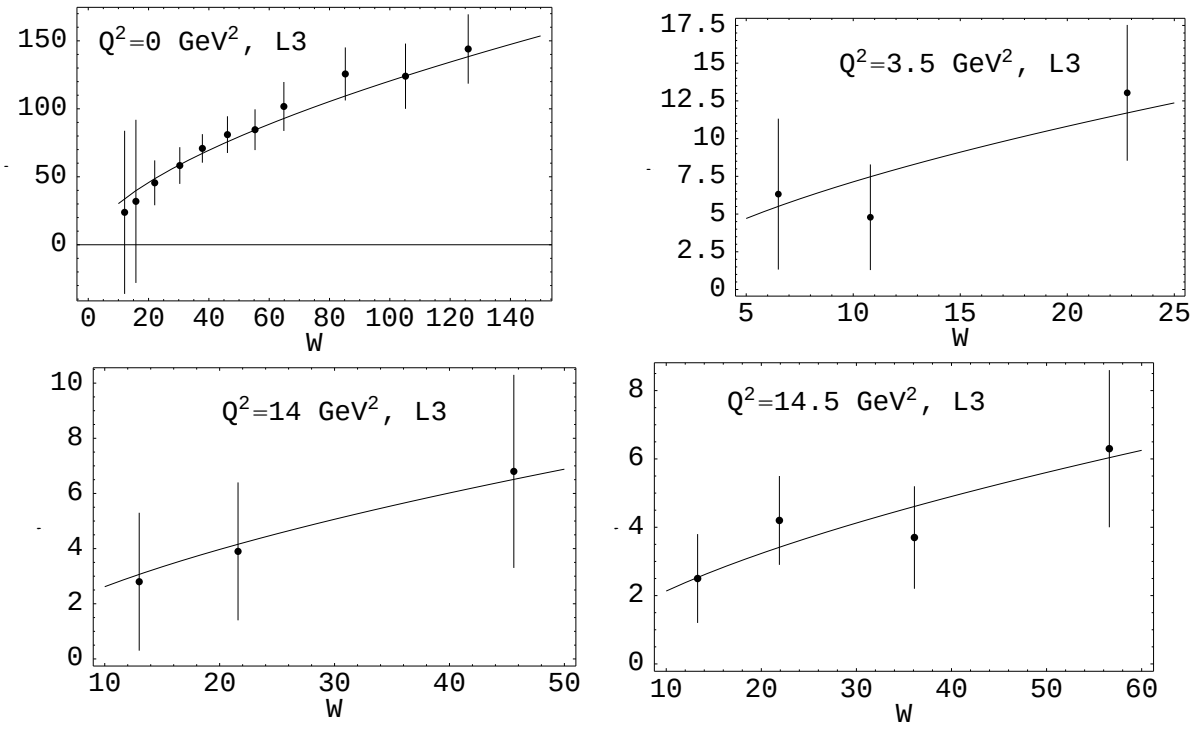

Figure 2: L3 data [41, 46] with the soft pomeron, reggeon, and fixed pole (box) contributions subtracted. The solid line is a fit of the form $A \times (W/GeV)^{0.6}$ with $A = 7.6, 1.8, 0.66, 0.54$ nb for $Q^2 = 0$, 3.5, 14, and 14.5 GeV^2 respectively.

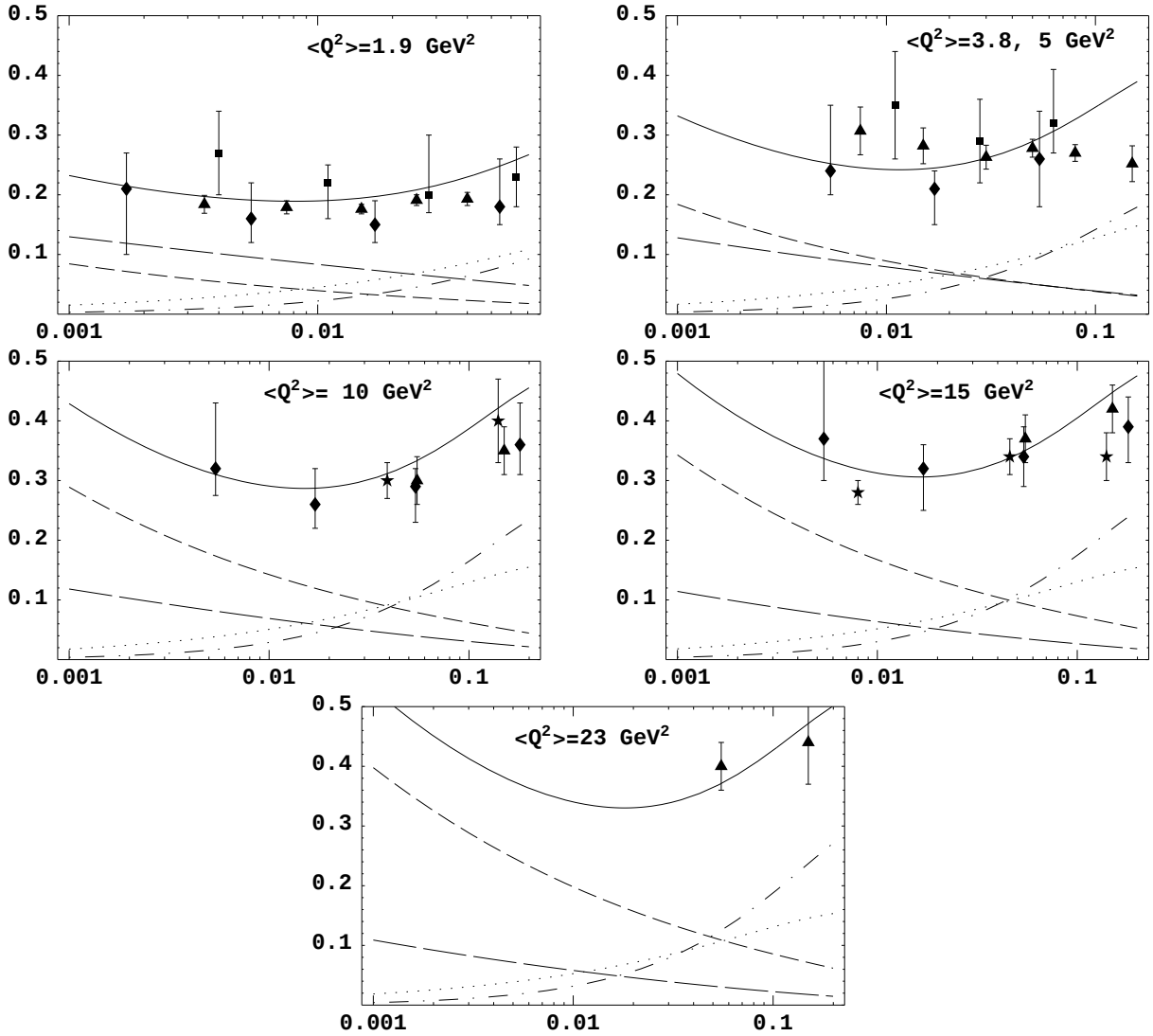

Figure 3: The photon structure function $F_2^\gamma(x, Q^2)$ as function of $x = \frac{Q^2}{W^2+Q^2}$. The data are: L3 [47], Triangles: OPAL [48], Boxes; OPAL [49], Diamonds: ALEPH [50, 51], Stars. The solid curve is our model without adjusted parameters. It consists of the following contributions: soft pomeron, long dashes; hard pomeron, short dashes; fixed pole, dot-dashes; reggeon, dots. The OPAL data in the $Q^2 = 5$ GeV^2 figure are at $\langle Q^2 \rangle = 3.8$GeV^2; the OPAL data in the $Q^2 = 15$ GeV^2 figure are at $\langle Q^2 \rangle = 17.6$GeV^2; and the ALEPH data in the $Q^2 = 15$ GeV^2 figure are at $\langle Q^2 \rangle = 14$GeV^2

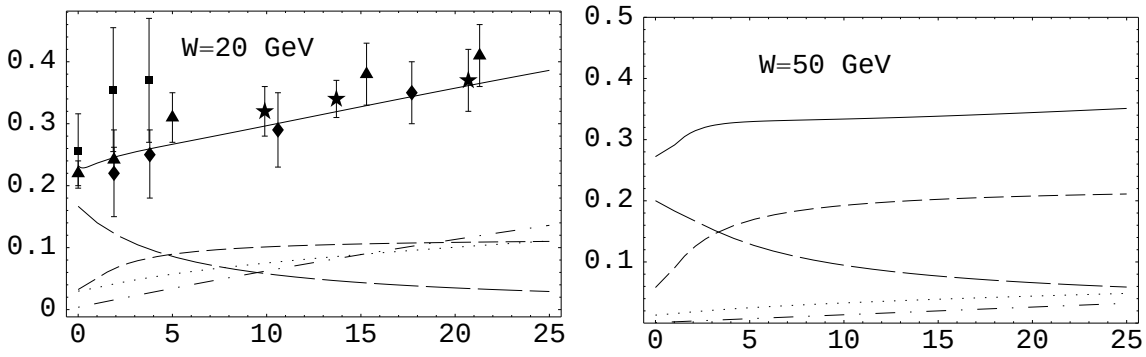

Figure 4: The modified photon structure function $\tilde{F}_2^\gamma = \frac{Q^2+0.6\mathrm{GeV}^2}{Q^2} * F_2^\gamma(x = \frac{Q^2}{W^2+Q^2}, Q^2)$ as function of Q^2 for $W \approx 20$ GeV and 50 GeV. The data are: L3 [47], Triangles: OPAL [48], Boxes; OPAL [49], Diamonds: ALEPH [50, 51], Stars. The solid curve is our model without adjusted parameters. It consists of the following contributions: soft pomeron, long dashes; hard pomeron, short dashes; fixed pole, dot-dashes; reggeon, dots.

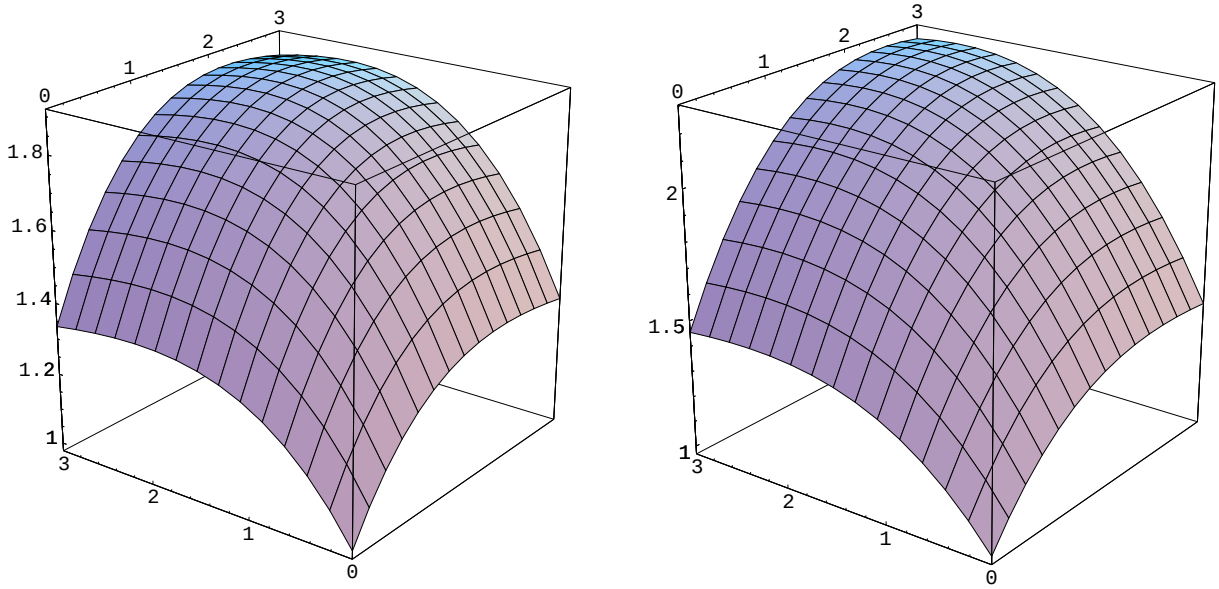

$W = 90$ GeV $\qquad\qquad$ $W = 245$ GeV

Figure 5: Ratio of the model cross section to the naive VMD cross section as a function of Q_i^2 for $0 \leq Q_i^2 \leq 3$ GeV^2, normalized to one at $Q^2 = 0$. The two plots are for the two centre of mass energies of the $\gamma^*\gamma^*$ system $W = 90$ GeV and $W = 245$ GeV.